ACS OMEGA

Open Access

http://pubs.acs.org/journal/acsodf

Article

PET and Optical Imaging of Caveolin-1 in Gastric Tumors

Sandeep Surendra Panikar, Shayla Shmuel, Jason S. Lewis, and Patrícia M. R. Pereira*

Cite This: *ACS Omega* 2023, 8, 35884−35892

Read Online

ACCESS | Metrics & More | Article Recommendations | Supporting Information

ABSTRACT: Previous studies have suggested tumoral caveolin-1 (CAV1) as a predictive biomarker for the response to anti-HER2 antibody drug therapies in gastric tumors. In this study, radiolabeled and fluorescently labeled anti-CAV1 antibodies were developed and tested as an immunoPET or optical imaging agent to detect CAV1 in HER2-positive/CAV1-high NCIN87 gastric tumors. The expression of CAV1 receptors in NCIN87 gastric tumors and nontumor murine organs was determined by Western blot. Binding assays were performed to validate the anti-CAV1 antibody specificity for CAV1-expressing NCIN87 cancer cells. Subcutaneous and orthotopic NCIN87 xenografts were used for PET imaging and *ex vivo* biodistribution of the radioimmunoconjugate. Additional HER2-PET and CAV1-optical imaging was also performed to determine CAV1 in the HER2-positive tumors. ^{89}Zr-labeled anti-CAV1 antibody was able to bind to CAV1-expressing NCIN87 cells with a B_{max} value of 2.7×10^3 CAV1 receptors/cell *in vitro*. ImmunoPET images demonstrated the localization of the antibody in subcutaneous NCIN87 xenografts. In the orthotopic model, CAV1 expression was also observed by optical imaging in the HER2-positive tumors previously imaged with HER2-PET. *Ex vivo* biodistribution analysis further confirmed these imaging results. The preclinical data from this study demonstrate the potential of using CAV1-PET and optical imaging for detecting gastric tumors.

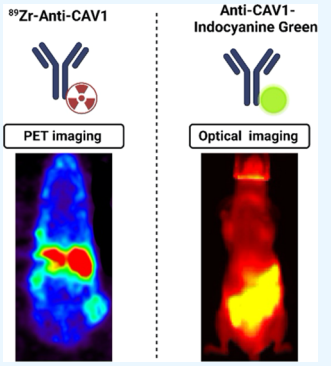

INTRODUCTION

Caveolin-1 (CAV1) is a membrane-associated protein that plays a complex role in cancer, functioning as both an oncogene and a tumor suppressor.[1] In the later stages of cancer development, overexpression of CAV1 associates with tumor cell progression, metastasis, and invasion.[2] However, a downregulation of CAV1 protein has been described for sarcomas, colon,[3] mammary,[4] and ovarian carcinomas.[5] In addition to its critical role in the structural formation of cholesterol-rich caveolae microdomains, CAV1 also participates in cholesterol transport, cell signaling, and the development of various diseases, including cardiovascular and metabolic diseases.[6]

Previous studies have demonstrated a negative correlation between tumoral CAV1 expression, membrane receptors, and the binding of antibody drugs to tumors.[7−12] Additional therapeutic studies demonstrated that tumoral CAV1 may play a role in reducing the effectiveness of antibody-based therapies in cancer treatment.[7,8,10,12,13] Gastric cancer cells containing high tumoral CAV1 show heterogeneous expression of membrane human epidermal growth factor receptor 2 (HER2), which results in low antibody-tumor binding.[7,13] Retrospective analyses of samples from HER2-overexpressing gastric cancer patients who underwent HER2-targeting Herceptin therapy suggest that patients with CAV1-high gastric cancers (immunohistochemistry, IHC 3+/2+; corresponding to 40% of the HER2-positive cancers) have reduced overall survival when compared with patients with CAV1-low cancers.[7] These previous CAV1 IHC and retrospective studies highlight the potential of CAV1 as a predictive biomarker for the tumor response to HER2-targeting antibody therapies.

Although we observed encouraging results using CAV1 IHC suggesting a role for CAV1 as a predictive biomarker to HER2-targeted antibody therapy,[7] IHC has several limitations that may reduce its ability as a clinical diagnostic.[14] Limitations to IHC include sampling bias, the inability to visualize the entire tumor tissue, or constraints due to tumor heterogeneity. Positron emission tomography (PET) is a highly sensitive and quantitative imaging modality that enables the noninvasive, real-time visualization of tumor biomarkers. Several tumor-targeted antibody PET agents have been developed and translated to date for applications in oncology.[15,16] ImmunoPET, a technology that combines the sensitivity of PET and the selectivity of antibodies, allows visualization of tumor biomarkers *in vivo*, and has the potential to be used as a complementary technique to IHC allowing for more accurate assessment of biomarkers in cancer diagnosis and treatment.[17,18]

Building on our previous work where we optimized the IHC detection of tumoral CAV1 using a murine CAV1-specific monoclonal antibody,[7] here we evaluated the utility of CAV1-targeted immunoPET to detect tumoral CAV1 in HER2-

Received: May 23, 2023
Accepted: September 5, 2023
Published: September 15, 2023

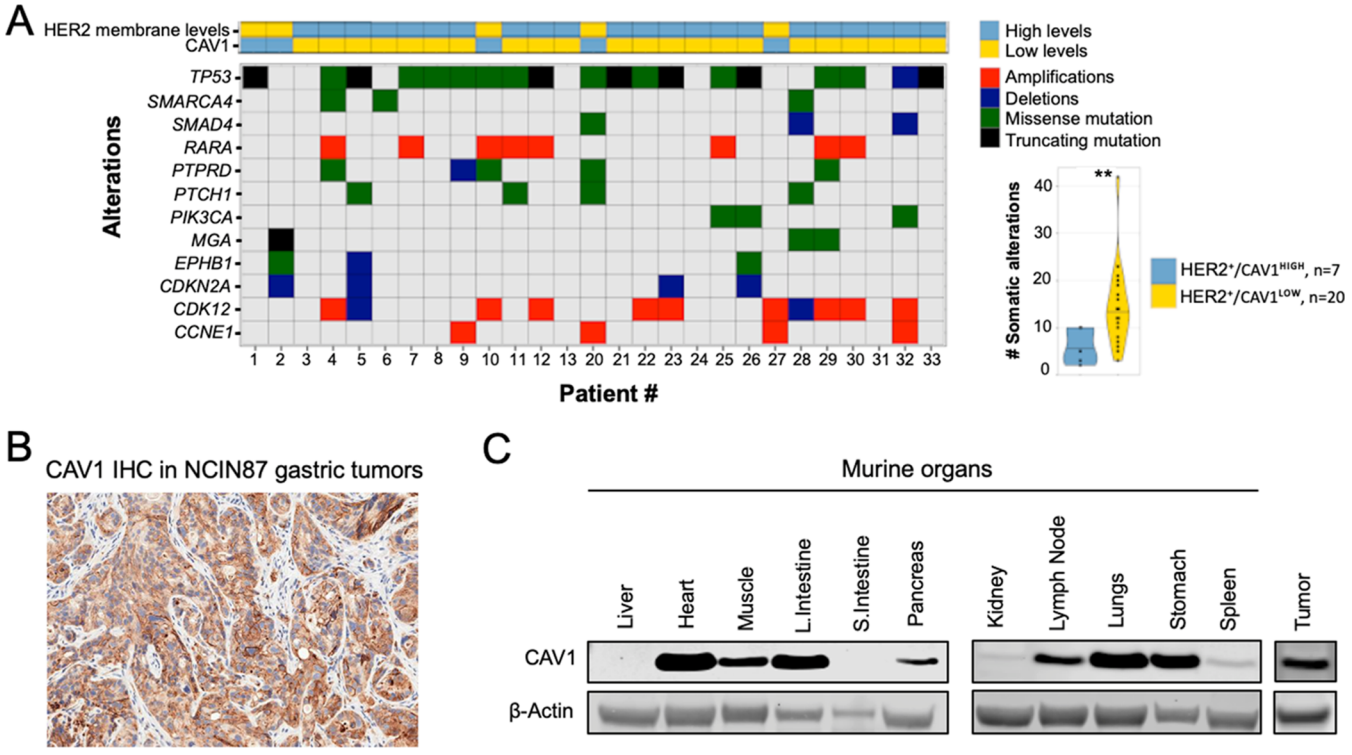

Figure 1. (A) Twelve most predominant genomic alterations present in CAV1-low versus CAV1-high HER2$^+$ gastric tumor tissues. HER2 membrane levels are classified as high versus low based on the quantification of immunofluorescence staining as described in Pereira et al. Nature Communications 2022.[7] Patients 1 to 33 are IDs for all HER2$^+$ gastric tumor tissues analyzed in the study. The graph on the right shows the number of genomic alterations, *EGFR* and *MET* amplification, and *PIK3CA* and *PTEN* mutations present in HER2$^+$CAV1^{LOW} versus HER2$^+$CAV1^{HIGH} gastric tumor tissues. HER2$^+$CAV1^{LOW} (n = 20) and HER2$^+$/CAV1^{HIGH} (n = 7). (B) Immunohistochemical (IHC) detection of CAV1 in NCIN87 tumors. (C) Western blot analyses of the CAV1 expression in NCIN87 xenografts and nontumor murine tissues (liver, heart, muscle, large intestine, small intestine, pancreas, kidney, lymph nodes, lungs, stomach, spleen, and tumor).

expressing gastric tumors. To further study the ability of CAV1-targeted imaging in gastric tumors, we also applied fluorescently labeled anti-CAV1 antibodies to investigate its distribution in an orthotopic model of HER2-expressing gastric tumors, allowing for a complementary visualization of tumoral CAV1 expression.

RESULTS

CAV1-High and CAV1-Low Gastric Tumors Have Distinct HER2 Signaling Profiles. Our previous studies in HER2-expressing gastric tumors demonstrated a negative relationship between tumoral CAV1 protein levels and antibody drug binding and efficacy.[7,13] High tumoral CAV1 associates with a lower tumor response to HER2-targeting antibody therapies when compared with tumors containing low levels of CAV1. Here, we analyzed genomic alterations in our previously reported cohort of patient-derived HER2-positive gastric tumor samples.[7] We used MSK-IMPACT data to determine somatic alterations in HER2$^+$/CAV1-low versus HER2$^+$/CAV1-high gastric cancer samples.[19,20] The most frequently altered genes in a cohort of 27 samples studied were *TP53*, *SMARCA4*, *RARA*, *PTPRD*, *PTCH1*, *PIK3CA*, *MGA*, *EPHB1*, *CDKN2A*, *CDK12*, and *CCNE1* (Figure 1A). Overall, CAV1-high gastric cancer samples exhibited a relatively low number of mutations compared with those of CAV1-low tumors. Taken together, our results suggest different signaling profiles in CAV1-high gastric cancer versus CAV1-low gastric cancer.

CAV1 Is Expressed in Tumors and Nontumor Tissues. Next, we determined CAV1 *ex vivo* expression in HER2$^+$ NCIN87 human gastric tumors and murine nontumor organs. IHC analyses demonstrated CAV1 reactivity at the membrane and cytoplasm of neoplastic cells and endothelial CAV1 reactivity in stromal blood vessels (Figure 1B). CAV1 was expressed at high protein levels in NCIN87 tumors (IHC 3+) as we have previously reported.[7] Additional Western blot analyses demonstrated high CAV1 protein levels in murine organs including the heart, large intestines, muscle, lungs, and nontumor stomach (Figure 1C, Supporting Information Figure 1). The high expression of CAV1 in murine organs is expected, as CAV1 is also highly expressed in those human organs according to data collected from the Human Protein Atlas database[21] (http://www.proteinatlas.org, Supporting Information Figure 2). These results show CAV1 expression in both gastric tumors and nontumor murine tissues.

[^{89}Zr]Zr-DFO-Anti-CAV1 Antibody Binds to CAV1-Expressing Gastric Cancer Cells. The anti-CAV1 antibody PET probe was developed by conjugating the anti-CAV1 antibody with the hexadentate chelator desferrioxamine (DFO) chelator and then radiolabeled with zirconium-89 (Supporting Information Figures 3−5 and Table 1). [^{89}Zr]Zr-DFO-anti-CAV1 was synthesized with a radiochemical purity, radiochemical yield, and specific activity of 96−98%, 95−99%, and 3.98 μCi/μg, respectively. *In vitro* studies demonstrated a positive correlation between the number of NCIN87 gastric cancer cells and the [^{89}Zr]Zr-DFO-anti-CAV1 antibody binding to cells (Figure 2A). It has been well explored that

https://doi.org/10.1021/acsomega.3c03614
ACS Omega 2023, 8, 35884−35892

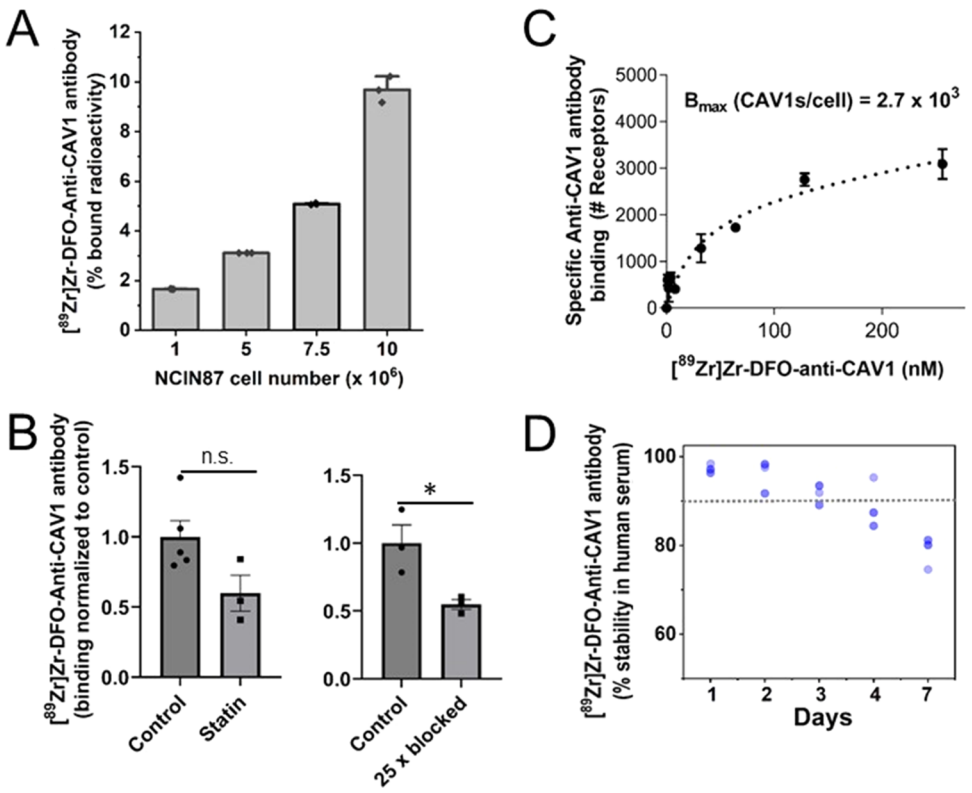

Figure 2. (A) ^{89}Zr-labeled anti-CAV1 antibody binding to CAV1-expressing NCIN87 gastric cancer cells. NCIN87 gastric cancer cells (1, 5, 7.5, or 10 million) were incubated with 37 KBq of [^{89}Zr]Zr-DFO-anti-CAV1 antibody (0.25−0.30 μg) for 1 h at room temperature. (B) Binding of the ^{89}Zr-labeled anti-CAV1 antibody in the absence or presence of an excess of unlabeled anti-CAV1 antibody or in the cells treated and not treated with lovastatin for 4 h. For the blocking study of ^{89}Zr-labeled anti-CAV1 antibody binding to cancer cells, cells were incubated with ^{89}Zr-labeled anti-CAV1 antibody in the presence of 25−30 μg DFO-Anti-CAV1. Data are presented as mean ± S.E.M., n = 3−5. (C) NCIN87 cells were incubated with the [^{89}Zr]Zr-DFO-anti-CAV1 antibody (0−256 nM) for 3 h at room temperature. Specific binding of [^{89}Zr]Zr-DFO-anti-CAV1 antibody and nonlinear regression curve fit are represented in black spheres and dotted lines. Data are presented as mean ± S.E.M., n = 5. (D) [^{89}Zr]Zr-DFO-anti-CAV1 antibody stability was determined in human serum for a period of 1 week. Radio-TLC chromatograms of the [^{89}Zr]Zr-DFO-anti-CAV1 antibody in human serum were run on silica strips using an eluent of 50 mM EDTA, pH 5.0. (*P < 0.05, n.s.= not significant; based on a Student's t test, n = 3−5)

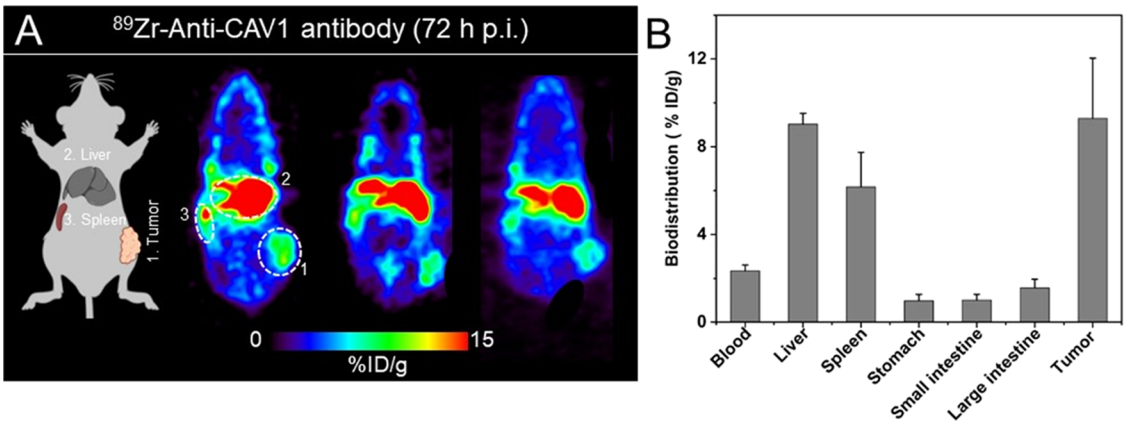

Figure 3. (A) Representative PET images at 72 h post tail vein injection of [^{89}Zr]Zr-DFO-anti-CAV1 antibody in mice bearing HER2-positive/CAV1-high NCIN87 xenografts. (B) Biodistribution profile at 72 h post injection of [^{89}Zr]Zr-DFO-anti-CAV1 antibody. The Supporting Information shows the full biodistribution.

lovastatin, a cholesterol-depleting drug, can significantly lower CAV1 expression in cancer cells.[7,13] The NCIN87 cells treated with lovastatin were incubated with [^{89}Zr]Zr-DFO-anti-CAV1 antibodies, and it was observed that the uptake in lovastatin-treated cells was reduced by ∼1.6-fold compared to the control (Figure 2B, left). Also in our binding study, [^{89}Zr]Zr-DFO-anti-CAV1 antibody uptake was ∼2.5-fold lower under blocking conditions compared with cells incubated with [^{89}Zr]Zr-DFO-anti-CAV1 antibody alone (Figure 2B, right). Additional competitive radioligand saturation-binding assays demonstrated that the NCIN87 gastric cancer cells express 2.7 × 10^3 CAV1 proteins/cell (Figure 2C and Supporting

https://doi.org/10.1021/acsomega.3c03614
ACS Omega 2023, 8, 35884−35892

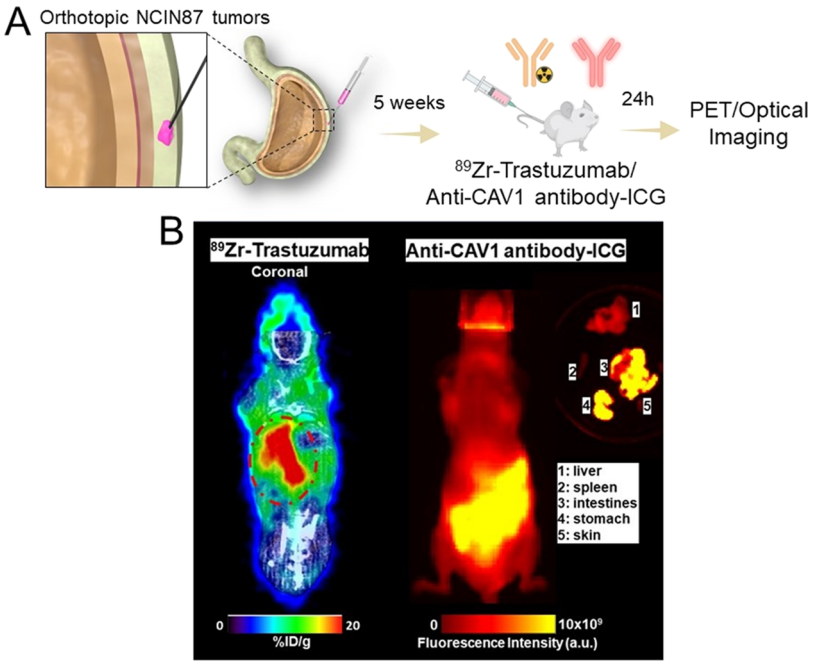

Figure 4. (A) Schematic representation of the intragastric injection method. (B) Dual-modality imaging of HER2 and CAV1 orthotopic models of gastric cancer. PET images and fluorescent images of trastuzumab (anti-HER2, left) and anti-CAV1 antibody (right) in an orthotopic model of NCIN87 gastric cancer. Left: Representative coronal and sagittal PET of trastuzumab in an orthotopic model of NCIN87 tumors. [^{89}Zr]Zr-DFO-trastuzumab (6.66−7.4 M 46 μg protein) was administered by tail vein injections, and PET images were acquired at 24 h post-injection. Scale bar represents %ID/g, percentage of injected dose per gram. Circles show trastuzumab uptake in the intestines and stomach. Right: Representative fluorescence images of uptake of anti-CAV1 antibody labeled with ICG. Images were acquired at 24 h after antibodies injection.

Information Figure 6) and that the antibody has moderate binding to the NCIN87 cancer cells with a K_D value of 108 nM. Additional serum stability analyses demonstrated that the [^{89}Zr]Zr-DFO-anti-CAV1 antibody radiotracer is stable for seven consecutive days in human serum (Figure 2D). Altogether, these data demonstrate that the [^{89}Zr]Zr-DFO-anti-CAV1 antibody is stable, and it binds CAV1-expressing gastric cancer cells.

ImmunoPET of CAV1-Expressing NCNIN87 Gastric Cancer Xenografts. Premised on our *in vitro* findings showing CAV1 expression in NCIN87 tumors (Figure 1) and anti-CAV1 antibody binding to cancer cells (Figure 2), we performed immunoPET imaging and a biodistribution study to monitor the ability of the anti-CAV1 antibody to accumulate in CAV1-positive NCIN87 subcutaneous tumors. PET images were acquired at 72 h post intravenous injection of [^{89}Zr]Zr-DFO-anti-CAV1 antibody. PET images demonstrated antibody accumulation in the tumor, heart, liver, spleen, with minimal uptake in the bones (Figure 3A and Supporting Information Figure 7), consistent with the biodistribution and clearance of full-length antibodies. To quantify the accumulation of the [^{89}Zr]Zr-DFO-anti-CAV1 antibody in murine tissues and NCIN87 tumors, we performed biodistribution studies at 72 h after antibody injection (Figure 3B). Here, we observed a percent-injected dose per gram (% ID/g) of 9.29 ± 2.74 in NCIN87 tumors. The uptake of the anti-CAV1 antibody was 9.6-fold higher in the subcutaneous NCIN87 tumors compared with the nontumor stomach tissues (0.97 ± 0.29% ID/g). Next, we performed the biodistribution studies with a blocking dose (100-fold of unlabeled anti-CAV1 antibody) to confirm the specificity of the radiolabeled anti-CAV1 antibody (Supporting Information Figure 8). A significant decrease (P = 0.0764) was observed in the binding of [^{89}Zr]Zr-DFO-anti-CAV1 antibody when the tumor was blocked with a 100-fold excess of unlabeled anti-CAV1 antibody. [^{89}Zr]Zr-DFO-anti-CAV1 antibody uptake in the NCIN87 tumors was 6-fold higher compared with the nonspecific IgG [^{89}Zr]Zr-DFO-IgG.[13] Collectively, these results demonstrate the ability of CAV1-targeted immunoPET to image gastric tumors.

CAV1-Targeted Optical Imaging in an Orthotopic Gastric Cancer Model. Next, we determined the potential for CAV1-targeted optical imaging in an orthotopic gastric cancer model (Figure 4A). The orthotopic gastric cancer model was developed by injecting NCIN87 gastric cancer cells into the subserosal layer of the stomach as previously described.[22] The development of HER2-positive NCIN87 tumors was confirmed by HER2-targeting immunoPET at 5 weeks after NCIN87 cancer cell injection in the stomach (Figure 4B). Once the tumors were identified, the mice were injected with fluorescently tagged (ICG) anti-CAV1 antibody for optical imaging. Protein staining using Coomassie blue was performed to detect the presence of anti-CAV1 labeled with ICG (Supporting Information Figure 9). Under nonreducing conditions, protein staining of the conjugated products exhibited bands similar to those of the unmodified anti-CAV1 antibody (Supporting Information Figure 9). Optical imaging was carried out at 24 h after injection of the anti-CAV1 antibody labeled with ICG. *Ex vivo* imaging studies demonstrated anti-CAV1 antibody uptake in the tumor stomach and intestines (Figure 4B). These results suggest the ability of CAV1-targeted optical imaging to detect primary gastric tumors and possible metastases in the intestines.

https://doi.org/10.1021/acsomega.3c03614
ACS Omega 2023, 8, 35884−35892

DISCUSSION

Previous studies have demonstrated a negative correlation between tumoral CAV1 and cell-surface HER2. In our previous work, we demonstrated that high protein levels of CAV1 in tumors were associated with low density of HER2 at the membrane of gastric cancer cells, low anti-HER2 antibody efficacy, and low survival in patients treated with trastuzumab.[7,13] These findings suggested that CAV1 could be a complementary biomarker to detect HER2 expression in tumors and a predictive biomarker for selecting tumors for anti-HER2 antibody therapies. In this study, we have developed radiolabeled and fluorescent anti-CAV1 antibodies and evaluated their potential to image gastric tumors using *in vivo* models. Specifically, we used HER2-positive/CAV1-expressing NCIN87 gastric cancer cells that were subcutaneously or orthotopically implanted in the stomachs of mice. Our results showed that these anti-CAV1 antibodies could potentially be used to image gastric tumors *in vivo*.

CAV1 is a structural protein of membrane caveolae that has both cancer-promoting[23] and anticancer effects.[24] CAV1 regulates proteins of the pro-survival phosphatidylinositol 3-kinase/Akt pathway and plays a role in the regulation of growth-factor-activated Ras-p42/44 mitogen-activated protein kinase (MAPK) pathway.[25] Previous studies have shown that an increase in CAV1 expression is associated with drug resistance in ovarian, colorectal, lung, head and neck, and gastric cancer cells.[7,13,26−30] Additionally, high expression of tumoral CAV1 has been linked to lower survival in patients with gastric cancer.[31] In our study, we found distinctive signaling profiles in CAV1-low versus CAV1-high gastric tumors in HER2-positive gastric tumors. Specifically, we observed *PIK3CA* mutations, as well as *EGFR*- and *MET*-amplification, which have been shown to determine clinical response to HER2-targeted therapies,[32] in CAV1-low gastric tumors.

Noninvasive PET imaging facilitates early assessment of tumor response to therapy in patients with HER2-positive gastric tumors. Previous studies have demonstrated the utility of HER2 immunoPET in detecting variations in HER2 expression, target engagement, and assessment of lesions in the whole body of patients with gastric tumors.[33,34] However, pretreatment HER2-PET with ^{89}Zr-labeled trastuzumab does not always correlate with tumor response to HER2-targeting antibody drugs.[35] Therefore, additional complementary techniques are needed to accurately assess the tumor response to therapy and guide treatment decisions in patients with HER2-positive gastric tumors.

Our PET imaging studies demonstrated that the radiolabeled anti-CAV1 antibody could delineate NCIN87 tumors. Although the density of CAV1 receptors on NCIN87 gastric cancer cells is lower (2700 CAV1 receptors per NCNI87 cancer cell) than that of other overexpressing receptors, such as HER2 (157,000 HER2 receptors per NCIN87 cancer cells),[13] we observed higher tumoral uptake of the ^{89}Zr-labeled anti-CAV1 antibody in NCIN87 tumors (9.29 ± 2.74% ID/g) compared to nontumor stomach tissue (0.97 ± 0.29% ID/g) or to a nonspecific IgG (<1.5% ID/g). However, the human/mouse cross-reactivity of the anti-CAV1 antibody used in our studies resulted in uptake not only in tumors but also in endogenous CAV1 expression in nontumor murine organs. To determine the potential imaging ability of this antibody, further optimization of the antibody binding to CAV1 and the use of other models of high CAV1 expression are needed. Since the level of cellular uptake of antibodies correlates with their affinity toward the targeted receptor, further studies are needed to optimize the affinity of the radiolabeled anti-CAV1 antibody toward CAV1 receptors.

In addition to determining CAV1-targeted imaging using a subcutaneous model, we established an orthotopic gastric cancer model using HER2-positive NCIN87 gastric cancer cells injected into the subserosa of the gastric body of nude mice. This method resulted in a tumor formation rate of 100%, similar to previous reports.[22] To confirm the development of HER2-positive NCIN87 tumors in mice, we used HER2-targeted immunoPET with the ^{89}Zr-labeled trastuzumab. We then prepared an optical imaging probe for targeting and imaging CAV1 tumors in the same mice by using ICG to label the anti-CAV1 antibody. The uptake of the ICG-conjugated anti-CAV1 antibody was observed in the tumor present in the stomach. Additional signal was observed in the intestines, which could indicate the ability of the gastric cancer model to metastasize into the intestines. Contrary to previous studies reporting liver uptake for ICG-labeled antibodies, we did not observe anti-CAV1 antibody uptake in the liver. Here, we validated CAV1 expression with optical imaging in HER2-positive tumors that were visualized with trastuzumab PET. However, a limitation of using an optical imaging probe is that it is challenging to detect deep tissue regions due to the absorption and scattering of light by tissues, leading to a decrease in signal intensity. Nevertheless, optical imaging has potential when used during endoscopy or surgery because activable optical probes can achieve relatively high signal-to-background ratios. Optical imaging can also be a low-cost, real-time imaging modality, which could help in the early detection of cancer and improve patient outcomes.

CONCLUSIONS

In this study, we radiolabeled a mouse/human cross-reactive anti-CAV1 antibody for immunoPET of CAV1-expressing gastric cancer cells. The ^{89}Zr-labeled anti-CAV1 antibody showed a high affinity for HER2-positive/CAV1-high NCIN87 gastric cancer cells, allowing visualization of gastric cancer cells growing subcutaneously and in murine stomachs. By combining PET and optical imaging, we validated CAV1 expression in the HER2-positive NCIN87 tumors. While this study shows promising results, future studies optimizing the CAV1 antibody, other CAV1-overexpressing models, and pre- versus post-therapy CAV1-PET imaging studies are necessary to fully validate the potential of CAV1 as a predictive biomarker of tumor response to HER2 therapies.

EXPERIMENTAL PROCEDURES

Cell Culture. The HER2-positive/CAV1-expressing human gastric cancer cells NCIN87 purchased from American Type Culture Collection were kept in culture using Roswell Park Memorial Institute-1640 growth medium supplemented with 10% (v/v) fetal serum bovine, 2 mM L-glutamine, 1 mM sodium pyruvate, 4.5 g/L glucose, 10 mM hydroxyethyl piperazineethanesulfonic acid, 1.5 g/L sodium bicarbonate, 100 U/mL penicillin, and 100 μg/mL streptomycin. NCIN87 gastric cancer cells used in this study were within passage 10.

Western Blot of Tissue Lysates. Whole-protein extracts were collected from liver, heart, muscle, large intestine, small intestine, pancreas, kidney, lymph nodes, lungs, stomach, and

https://doi.org/10.1021/acsomega.3c03614
ACS Omega 2023, 8, 35884−35892

spleen nontumor tissues of *nu/nu* female mice. Additional whole-protein extracts were collected from the NCIN87 tumors. Tissue lysates were prepared in radioimmunoprecipitation assay buffer, and the Pierce BCA Protein Assay Kit (Thermo Fisher Scientific) was used to quantify protein in tissue lysates. Protein electrophoresis was performed using NuPage 4−12% Bis-Tris protein gels (Invitrogen). Proteins were transferred to polyvinylidene difluoride membranes (Bio-Rad). After membrane blocking in 5% w/v milk (Bio-Rad), membranes were probed with mouse anti-β-actin 1:20,000 (Sigma, A1978) or rabbit anti-CAV1 1:500 (Abcam, ab2910). After washing the membranes with TBS-T, the membranes were incubated with IRDye 800CW antirabbit or antimouse IgG 1:15,000 (LI-COR Biosciences) and imaged on the Odyssey Infrared Imaging System (LI-COR Biosciences).

Conjugation and Radiolabeling of Anti-CAV1 Antibody with Zirconium-89. ^{89}Zr-oxalate was obtained from the Washington School of Medicine at St. Louis or Memorial Sloan Kettering Cancer Center isotope production teams. To prepare [^{89}Zr]Zr-DFO-anti-CAV1, an anti-CAV1 antibody (anti-CAV1, BD Biosciences, 610407) was first conjugated with the bifunctional chelate *p*-isothiocyanatobenzyl-desferrioxamine (DFO-Bz-NCS; Macrocyclics) and then labeled with zirconium-89 (^{89}Zr). The DFO-conjugated anti-CAV1-antibody was characterized using MALDI mass spectrometry analyses and gel electrophoresis (Supporting Information Figures 3 and 4 and Table 1). The [^{89}Zr]Zr-DFO-anti-CAV1 antibody conjugates had a radiochemical purity of 98%, radiochemical yields ranging from 96 to 98% (Supporting Information Figure 5), and specific activities of 3.98 μCi/μg. Binding studies of the [^{89}Zr]Zr-DFO-anti-CAV1 conjugate were performed using the HER2-positive/CAV1-expressing NCIN87 cancer cells prior to *in vivo* experimentation. [^{89}Zr]Zr-DFO-anti-CAV1 stability was above 85% after incubation in human serum (Sigma-Aldrich) at 37 °C for a period of 96 h.

Anti-CAV1 Antibody Labeling with ICG. Conjugation of anti-CAV1 antibody (BD Biosciences, 610407) with Indocyanine Green (ICG) was performed at a molar ratio of 1:6 (antibody:ICG) in 0.1 M disodium phosphate (Na_2HPO_4, pH 8.6) at room temperature for 1.5 h. The ICG-labeled antibody was purified with a size exclusion column (PD-10; GE Healthcare, Piscataway, NJ). The concentration of ICG was calculated by measuring the absorption with a UV−vis system to confirm the number of fluorophore molecules conjugated with each antibody molecule. The antibody concentration was also determined by measuring the absorption at 280 nm with a UV−vis system and confirmed by nanodrop's protein measurement. To confirm the conjugation of ICG to anti-CAV1 antibody, the conjugate was analyzed by SDS−PAGE, and the gel was imaged using the Odyssey Infrared Imaging System (LI-COR Biosciences, Supporting Information Figure 9).

Binding, Saturation-Binding, and Blocking Assays. For the binding assays, the HER2-positive/CAV1-expressing NCIN87 cancer cells were incubated with 37 kBq of ^{89}Zr-labeled anti-CAV1 antibody (1 μg) for 1 h at 37 °C. Blocking experiments were performed by incubating NCIN87 cancer cells with the zirconium-89 labeled antibody in the presence of a 25-fold excess (25 μg) of unlabeled DFO-conjugated anti-CAV1 antibody. Cholesterol-depleting drug lovastatin has been shown to reduce the CAV1 expression in the gastric cancer model.[13,36] The CAV1-expressing NCIN87 cells were treated with lovastatin for 4 h, followed by incubation with ^{89}Zr-labeled anti-CAV1 antibody (37 kBq, 1 μg) for 1 h at room temperature. The radioactivity from the supernatants and the cell pellet was then measured with a gamma counter, and the immunoreactivity was calculated by dividing the radioactivity measured in the cell pellet by the sum of the radioactivity in the cell pellet plus washing fractions.

For the saturation-binding assays, NCIN87 cells were incubated with [^{89}Zr]Zr-DFO-anti-CAV1 (0−256 nM) in PBS (pH 7.5) containing 1% (m/v) bovine serum albumin (Sigma) and 1% (m/v) sodium azide (Acros Organics) for 2.5 h at 4 °C. Unbound radioactivity was removed, and cells were washed three times with PBS. The cells were collected using a solution of 100 mM sodium hydroxide (NaOH), and the total cell-bound radioactivity was measured on a gamma counter. Total binding was plotted versus the concentration of the [^{89}Zr]Zr-DFO-anti-CAV1 antibody. To calculate B_{max}, K_D, and the nonspecific binding component, the results were fit via nonlinear regression with a one-site binding model in GraphPad Prism 9. The ^{89}Zr-IgG (Sigma-Aldrich) nonspecific component was subtracted from the total binding to generate specific binding curves.

Subcutaneous Tumor Implantation. Animal experiments were performed following the guidelines approved by the Research Animal Resource Center and Institutional Animal Care and Use Committee at the Washington School of Medicine at St. Louis or Memorial Sloan Kettering Cancer Center. The HER2-positive/CAV1-expressing NCIN87 cells (5 million) were injected subcutaneously (200 μL containing 1:1 (v/v) cell media and basement membrane Matrigel, BD matrigel, BD Biosciences) in the right flank of eight- to 10-week-old *nu/nu* female mice (Charles River Laboratories). NCIN87 tumors were allowed to grow until they reached approximately 150−250 mm^3 in volume, as measured by an external vernier caliper and applying the equation $V = (4\pi/3) \times (\alpha/2)^2 \times (b/2)$. V is the tumor volume (mm^3), α is the longest axis (mm), and b is the axis perpendicular to the longest axis (mm).

Orthotopic Tumor Implantation. Gastric orthotopic models were developed by injection of NCIN87 cells into the serous membrane of the stomach of *nu/nu* female mice.[22] The mice were anesthetized by inhalation of 1−2% isofluorane in an oxygen gas mixture and kept on a heated platform during surgical procedures. Meloxicam (2.0 mg/kg of mice) was administered subcutaneously during the perioperative period. A solution of 0.25% bupivacaine was administrated by intradermal injection in the area surrounding the incision line. The abdomen was swabbed with sterile 70% ethanol alcohol pads followed by a povidone-iodine (Betadine) scrub. A small longitudinal incision (0.5 to 1 cm in length) was performed in the skin and peritoneum; the stomach was identified, and NCIN87 cells (5 million) in 30 μL containing 1:1 (v/v) cell media and basement membrane matrigel (BD Matrigel, BD Biosciences) were injected into the serous membrane of the stomach. The injection site was gently pressed with a sterile cotton swab to prevent cell leakage. After cell injection, the stomach was replaced in the abdomen. The abdominal and skin incisions were closed with 4−0 Vicryl sutures (Fischer Scientific) and sterile 9 mm wound clips, respectively. The mice were injected with a warmed saline solution (10 mL/kg of mice) to facilitate rehydration and recovery from anesthesia. Buprenorphine 0.25% was administered before recovery, and dosages of 10 μL were repeated

https://doi.org/10.1021/acsomega.3c03614
ACS Omega 2023, 8, 35884−35892

(total of 100 μL) postsurgery, as needed, every 4−6 h. The mice were monitored for any signs of pain and distress. The mice were subsequently used for PET imaging and optical imaging 5 weeks after the cell's inoculation.

CAV1 Immunohistochemistry (IHC) in NCIN87 Tumors. IHC of CAV1 protein levels in NCIN87 tumors was performed using an anti-CAV1 BD Biosciences antibody (610407) as previously described.[7] Briefly, the primary anti-CAV1 antibody 1:250 (v/v) was applied in NCIN87 tumors, followed by incubation with the antimouse secondary antibody (DS9800, Novocastra Bond Polymer Refine Detection, Leica Biosystems).

Biodistribution Studies and Small-Animal Positron Emission Tomography (PET). [^{89}Zr]Zr-DFO-anti-CAV1 (6.66−7.4 MBq, 41−46 μg protein) was administered by intravenous injection, and PET images were acquired at 72 h post injection. PET imaging experiments were conducted on a microPET Focus 120 scanner (Concorde Microsystems). For the blocking study, 100 μg of the anti-CAV1 antibodies was injected intravenously prior to the injection of [^{89}Zr]Zr-DFO-anti-CAV1 (0.147 Mbq, 1 μg protein). Acute biodistribution studies were performed 72 h after injection of the [^{89}Zr]Zr-DFO-anti-CAV1 antibody. The mice were sacrificed, and organs were harvested, weighed, and assayed in the gamma counter for biodistribution studies. Radioactivity associated with each organ was expressed as a percentage of injected dose per gram of organ (% ID/g).

^{89}Zr-Labeled Trastuzumab PET Imaging and Anti-CAV1 Antibody-ICG Optical Imaging. Mice bearing orthotopic NCIN87 tumors were intravenously coadministered [^{89}Zr]Zr-DFO-trastuzumab (7.03−7.77 MBq, 47.5−52.5 μg protein) and ICG-labeled anti-CAV1 antibody (20 nM). PET imaging experiments were conducted on a microPET Focus 120 scanner (Concorde Microsystems) 24 h after injection of ^{89}Zr-DFO-trastuzumab. Following PET imaging, optical imaging was conducted using an IVIS Spectrum imaging system (PerkinElmer; excitation wavelength 745 nm and emission wavelength 840 nm) and data were analyzed with Living Image software version 4.1 (PerkinElmer). After imaging, the mice were sacrificed and *ex vivo* optical imaging was performed on liver, stomach, spleen, intestines, and skin.

Statistical Analyses. Data are expressed as mean ± SEM. Groups and data sets were compared using the Student *t*-test using GraphPad Prism 9.00 (www.graphpad.com) or OriginPro 2023b (www.originlab.com). In biodistribution and imaging studies, each cohort included three mice per biodistribution time point.

■ ASSOCIATED CONTENT

Supporting Information

The Supporting Information is available free of charge at https://pubs.acs.org/doi/10.1021/acsomega.3c03614.

MALDI analysis, SDS gel, radio-TLC chromatograms, UV−vis and SDS-PAGE of the ICG-labeled anti-CAV1 antibody, raw data of Western blot, CAV1 expression on mice organs, saturation-binding assay, biodistribution analysis of mice organs, and degree of labeling of anti-CAV1 (Table 1) (PDF)

■ AUTHOR INFORMATION

Corresponding Author

Patrícia M. R. Pereira − *Department of Radiology, Mallinckrodt Institute of Radiology, Washington University School of Medicine, St. Louis, Missouri 63110, United States;* orcid.org/0000-0002-4772-9339; Phone: +1 314-273-4898; Email: ribeiropereirap@wustl.edu

Authors

Sandeep Surendra Panikar − *Department of Radiology, Mallinckrodt Institute of Radiology, Washington University School of Medicine, St. Louis, Missouri 63110, United States*

Shayla Shmuel − *Department of Radiology, Mallinckrodt Institute of Radiology, Washington University School of Medicine, St. Louis, Missouri 63110, United States*

Jason S. Lewis − *Department of Radiology, Memorial Sloan Kettering Cancer Center, New York, New York 10065, United States; Department of Pharmacology and Department of Radiology, Weill Cornell Medical College, New York, New York 10065, United States; Molecular Pharmacology Program and Radiochemistry and Molecular Imaging Probes Core, Memorial Sloan Kettering Cancer Center, New York, New York 10065, United States;* orcid.org/0000-0001-7065-4534

Complete contact information is available at: https://pubs.acs.org/10.1021/acsomega.3c03614

Funding

This research was supported by internal funds provided by the Mallinckrodt Institute of Radiology, NIH (R01 CA244233−01A1), and in part by American Cancer Society (IRG-21−133−64−03). P.M.R.P. acknowledges NIH (R01 CA244233−01A1 and 1R37CA27649801), the Breast Cancer Alliance, the Elsa Pardee Foundation, the Alvin J. Siteman Cancer Center through The Foundation for Barnes-Jewish Hospital, and the National Cancer Institute (P30 CA091842). The content is solely the responsibility of the authors and does not necessarily represent the official views of the National Institutes of Health. J.S.L. acknowledges NIH NCI R35CA232130 and NIH R01 CA244233−01A1. The Preclinical Imaging Facility at Washington University School of Medicine in St. Louis was supported by NIH/NCI Siteman Cancer Center (SCC) Support Grant P30 CA091842, NIH instrumentation grants S10OD018515 and S10OD030403, and internal funds provided by Mallinckrodt Institute of Radiology.

Notes

The authors declare no competing financial interest.

■ ACKNOWLEDGMENTS

The authors thank the Washington University isotope production team for the production of zirconium-89 and the small-animal imaging facility for helping with the small-animal PET/CT data generation. They also acknowledge the MSK Small-Animal Imaging Core Facility, the MSK Radiochemistry and Molecular Imaging Probe Core, and the MSK Antitumor Assessment Core and Molecular Cytology Core Facility, which were supported by NIH grant P30 CA08748. The authors are thankful to Dr. Luis Batista for letting us use the Odyssey Infrared Imaging System. They are grateful to Dr. Elisa De Stanchina and the team at the Antitumor Assessment Core at Memorial Sloan Kettering Cancer Center for helping with the MSK-IMPACT data on the patient-derived xenograft samples.

REFERENCES

(1) Quest, A.F.G.; Lobos-González, L.; Nuñez, S.; Sanhueza, C.; Fernández, J. G.; Aguirre, A.; Rodríguez, D.; Leyton, L.; Torres, V. The caveolin-1 connection to cell death and survival. *Curr. Mol. Med.* **2013**, *13* (2), 266−281, DOI: 10.2174/156652413804810745.

(2) Campos, A.; Burgos-Ravanal, R.; González, M. F.; Huilcaman, R.; Lobos González, L.; Quest, A. F. Cell Intrinsic and Extrinsic Mechanisms of Caveolin-1-Enhanced Metastasis. *Biomolecules* **2019**, *9*, No. 314, DOI: 10.3390/biom9080314.

(3) Bender, F. C.; Reymond, M. A.; Bron, C.; Quest, A. F. G. Caveolin-1 Levels Are Down-Regulated in Human Colon Tumors, and Ectopic Expression of Caveolin-1 in Colon Carcinoma Cell Lines Reduces Cell Tumorigenicity1. *Cancer Res.* **2000**, *60* (20), 5870−5878.

(4) Lee, S. W.; Reimer, C. L.; Oh, P.; Campbell, D. B.; Schnitzer, J. E. Tumor cell growth inhibition by caveolin re-expression in human breast cancer cells. *Oncogene* **1998**, *16* (11), 1391−1397.

(5) Wiechen, K.; Diatchenko, L.; Agoulnik, A.; Scharff, K. M.; Schober, H.; Arlt, K.; Zhumabayeva, B.; Siebert, P. D.; Dietel, M.; Schäfer, R.; Sers, C. Caveolin-1 is down-regulated in human ovarian carcinoma and acts as a candidate tumor suppressor gene. *Am. J. Pathol.* **2001**, *159* (5), 1635−1643.

(6) Liu, P.; Rudick, M.; Anderson, R. G. Multiple functions of caveolin-1. *J. Biol. Chem.* **2002**, *277* (44), 41295−41298.

(7) Pereira, P. M. R.; Mandleywala, K.; Monette, S.; Lumish, M.; Tully, K. M.; Panikar, S. S.; Cornejo, M.; Mauguen, A.; Ragupathi, A.; Keltee, N. C.; Mattar, M.; Janjigian, Y. Y.; Lewis, J. S. Caveolin-1 temporal modulation enhances antibody drug efficacy in heterogeneous gastric cancer. *Nat. Commun.* **2022**, *13* (1), No. 2526.

(8) Sekhar, S. C.; Kasai, T.; Satoh, A.; Shigehiro, T.; Mizutani, A.; Murakami, H.; El-Aarag, B. Y.; Salomon, D. S.; Massaguer, A.; de Llorens, R.; Seno, M. Identification of caveolin-1 as a potential causative factor in the generation of trastuzumab resistance in breast cancer cells. *J. Cancer* **2013**, *4* (5), 391−401.

(9) Chung, Y.-C.; Chang, C.-M.; Wei, W.-C.; Chang, T.-W.; Chang, K.-J.; Chao, W.-T. Metformin-induced caveolin-1 expression promotes T-DM1 drug efficacy in breast cancer cells. *Sci. Rep.* **2018**, *8* (1), No. 3930.

(10) Sung, M.; Tan, X.; Lu, B.; Golas, J.; Hosselet, C.; Wang, F.; Tylaska, L.; King, L.; Zhou, D.; Dushin, R.; Myers, J. S.; Rosfjord, E.; Lucas, J.; Gerber, H. P.; Loganzo, F. Caveolae-Mediated Endocytosis as a Novel Mechanism of Resistance to Trastuzumab Emtansine (T-DM1). *Mol. Cancer Ther.* **2018**, *17* (1), 243−253.

(11) Park, S. S.; Kim, J. E.; Kim, Y. A.; Kim, Y. C.; Kim, S. W. Caveolin-1 is down-regulated and inversely correlated with HER2 and EGFR expression status in invasive ductal carcinoma of the breast. *Histopathology* **2005**, *47* (6), 625−630.

(12) Indira Chandran, V.; Månsson, A. S.; Barbachowska, M.; Cerezo-Magaña, M.; Nodin, B.; Joshi, B.; Koppada, N.; Saad, O. M.; Gluz, O.; Isaksson, K.; Borgquist, S.; Jirström, K.; Nabi, I. R.; Jernström, H.; Belting, M. Hypoxia Attenuates Trastuzumab Uptake and Trastuzumab-Emtansine (T-DM1) Cytotoxicity through Redistribution of Phosphorylated Caveolin-1. *Mol. Cancer Res.* **2020**, *18* (4), 644−656.

(13) Pereira, P. M. R.; Sharma, S. K.; Carter, L. M.; Edwards, K. J.; Pourat, J.; Ragupathi, A.; Janjigian, Y. Y.; Durack, J. C.; Lewis, J. S. Caveolin-1 mediates cellular distribution of HER2 and affects trastuzumab binding and therapeutic efficacy. *Nat. Commun.* **2018**, *9* (1), No. 5137.

(14) Kim, S. W.; Roh, J.; Park, C. S. Immunohistochemistry for Pathologists: Protocols, Pitfalls, and Tips. *J. Pathol. Transl. Med.* **2016**, *50* (6), 411−418.

(15) Wei, W.; Rosenkrans, Z. T.; Liu, J.; Huang, G.; Luo, Q. Y.; Cai, W. ImmunoPET: Concept, Design, and Applications. *Chem. Rev.* **2020**, *120* (8), 3787−3851.

(16) Manafi-Farid, R.; Ataeinia, B.; Ranjbar, S.; Jamshidi Araghi, Z.; Moradi, M. M.; Pirich, C.; Beheshti, M. ImmunoPET: Antibody-Based PET Imaging in Solid Tumors. *Front. Med.* **2022**, *9*, No. 916693.

(17) Kist de Ruijter, L.; van de Donk, P. P.; Hooiveld-Noeken, J. S.; Giesen, D.; Elias, S. G.; Lub-de Hooge, M. N.; Oosting, S. F.; Jalving, M.; Timens, W.; Brouwers, A. H.; Kwee, T. C.; Gietema, J. A.; Fehrmann, R. S. N.; Fine, B. M.; Sanabria Bohórquez, S. M.; Yadav, M.; Koeppen, H.; Jing, J.; Guelman, S.; Lin, M. T.; Mamounas, M. J.; Eastham, J. R.; Kimes, P. K.; Williams, S. P.; Ungewickell, A.; de Groot, D. J. A.; de Vries, E. G. E. Whole-body CD8(+) T cell visualization before and during cancer immunotherapy: a phase 1/2 trial. *Nat. Med.* **2022**, *28* (12), 2601−2610.

(18) Chegu, A.; Panikar, S. S.; Pereira, P. M. R. Mini-review: Antibody-PET of receptor tyrosine kinase interplay and heterogeneity. *Nucl. Med. Biol.* **2022**, *108*−*109*, 70−75.

(19) Chen, K.; Ahmed, S.; Adeyi, O.; Dick, J. E.; Ghanekar, A. Human solid tumor xenografts in immunodeficient mice are vulnerable to lymphomagenesis associated with Epstein-Barr virus. *PLoS One* **2012**, *7* (6), No. e39294.

(20) Wetterauer, C.; Vlajnic, T.; Schüler, J.; Gsponer, J. R.; Thalmann, G. N.; Cecchini, M.; Schneider, J.; Zellweger, T.; Pueschel, H.; Bachmann, A.; Ruiz, C.; Dirnhofer, S.; Bubendorf, L.; Rentsch, C. A. Early development of human lymphomas in a prostate cancer xenograft program using triple knock-out immunocompromised mice. *Prostate* **2015**, *75* (6), 585−592.

(21) Uhlen, M.; Oksvold, P.; Fagerberg, L.; Lundberg, E.; Jonasson, K.; Forsberg, M.; Zwahlen, M.; Kampf, C.; Wester, K.; Hober, S.; Wernerus, H.; Björling, L.; Ponten, F. Towards a knowledge-based Human Protein Atlas. *Nat. Biotechnol.* **2010**, *28* (12), 1248−1250.

(22) Busuttil, R. A.; Liu, D. S.; Di Costanzo, N.; Schröder, J.; Mitchell, C.; Boussioutas, A. An orthotopic mouse model of gastric cancer invasion and metastasis. *Sci. Rep* **2018**, *8* (1), No. 825.

(23) Galbiati, F.; Volonte, D.; Engelman, J. A.; Watanabe, G.; Burk, R.; Pestell, R. G.; Lisanti, M. P. Targeted downregulation of caveolin-1 is sufficient to drive cell transformation and hyperactivate the p42/44 MAP kinase cascade. *EMBO J.* **1998**, *17* (22), 6633−6648.

(24) Park, J.; Bae, E.; Lee, C.; Yoon, S. S.; Chae, Y. S.; Ahn, K. S.; Won, N. H. RNA interference-directed caveolin-1 knockdown sensitizes SN12CPM6 cells to doxorubicin-induced apoptosis and reduces lung metastasis. *Tumour Biol.* **2010**, *31* (6), 643−650.

(25) Wang, X.; Feng, S.; Zhang, H.; Wang, Y.; Cui, Y.; Wang, Z.; Liu, J.; Zou, W. RNA inference-mediated caveolin-1 down-regulation decrease estrogen receptor alpha (ERα) signaling in human mammary epithelial cells. *Mol. Biol. Rep* **2011**, *38* (2), 761−768.

(26) Zou, W.; Ma, X.; Hua, W.; Chen, B.; Cai, G. Caveolin-1 mediates chemoresistance in cisplatin-resistant ovarian cancer cells by targeting apoptosis through the Notch-1/Akt/NF-κB pathway. *Oncol. Rep.* **2015**, *34* (6), 3256−3263.

(27) Li, Z.; Wang, N.; Huang, C.; Bao, Y.; Jiang, Y.; Zhu, G. Downregulation of caveolin-1 increases the sensitivity of drug-resistant colorectal cancer HCT116 cells to 5-fluorouracil. *Oncol. Lett.* **2017**, *13* (1), 483−487.

(28) Han, F.; Zhang, L.; Zhou, Y.; Yi, X. Caveolin-1 regulates cell apoptosis and invasion ability in paclitaxel-induced multidrug-resistant A549 lung cancer cells. *Int. J. Clin. Exp. Pathol.* **2015**, *8* (8), 8937−8947.

(29) Wang, X.; Lu, B.; Dai, C.; Fu, Y.; Hao, K.; Zhao, B.; Chen, Z.; Fu, L. Caveolin-1 Promotes Chemoresistance of Gastric Cancer Cells to Cisplatin by Activating WNT/β-Catenin Pathway. *Front. Oncol.* **2020**, *10*, No. 46.

(30) Bouhaddou, M.; Lee, R. H.; Li, H.; Bhola, N. E.; O'Keefe, R. A.; Naser, M.; Zhu, T. R.; Nwachuku, K.; Duvvuri, U.; Olshen, A. B.; Roy, R.; Hechmer, A.; Bolen, J.; Keysar, S. B.; Jimeno, A.; Mills, G. B.; Vandenberg, S.; Swaney, D. L.; Johnson, D. E.; Krogan, N. J.; Grandis, J. R. Caveolin-1 and Sox-2 are predictive biomarkers of cetuximab response in head and neck cancer. *JCI Insight* **2021**, *6* (20), No. e151982, DOI: 10.1172/jci.insight.151982.

(31) Li, J. H.; Liu, S.; Zhou, H.; Qu, L. H.; Yang, J. H. starBase v2.0: decoding miRNA-ceRNA, miRNA-ncRNA and protein-RNA interaction networks from large-scale CLIP-Seq data. *Nucleic Acids Res.* **2014**, *42* (Database issue), No. D92−7.

https://doi.org/10.1021/acsomega.3c03614
ACS Omega 2023, 8, 35884−35892

(32) Filho, O. M.; Viale, G.; Stein, S.; Trippa, L.; Yardley, D. A.; Mayer, I. A.; Abramson, V. G.; Arteaga, C. L.; Spring, L. M.; Waks, A. G.; Wrabel, E.; DeMeo, M. K.; Bardia, A.; Dell'Orto, P.; Russo, L.; King, T. A.; Polyak, K.; Michor, F.; Winer, E. P.; Krop, I. E. Impact of HER2 Heterogeneity on Treatment Response of Early-Stage HER2-Positive Breast Cancer: Phase II Neoadjuvant Clinical Trial of T-DM1 Combined with Pertuzumab. *Cancer Discovery* **2021**, *11* (10), 2474−2487.
(33) O'Donoghue, J. A.; Lewis, J. S.; Pandit-Taskar, N.; Fleming, S. E.; Schöder, H.; Larson, S. M.; Beylergil, V.; Ruan, S.; Lyashchenko, S. K.; Zanzonico, P. B.; Weber, W. A.; Carrasquillo, J. A.; Janjigian, Y. Y. Pharmacokinetics, Biodistribution, and Radiation Dosimetry for (89)Zr-Trastuzumab in Patients with Esophagogastric Cancer. *J. Nucl. Med.* **2018**, *59* (1), 161−166.
(34) Lumish, M. A.; Maron, S. B.; Paroder, V.; Chou, J. F.; Capanu, M.; Philemond, S.; O'Donoghue, J. A.; Schöder, H.; Lewis, J. S.; Lyashchenko, S. K.; Pandit-Taskar, N.; Janjigian, Y. Y. Noninvasive Assessment of Human Epidermal Growth Factor Receptor 2 (HER2) in Esophagogastric Cancer Using (89)Zr-Trastuzumab PET: A Pilot Study. *J. Nucl. Med.* **2023**, *64* (5), 724−730.
(35) Gebhart, G.; Lamberts, L. E.; Wimana, Z.; Garcia, C.; Emonts, P.; Ameye, L.; Stroobants, S.; Huizing, M.; Aftimos, P.; Tol, J.; Oyen, W. J.; Vugts, D. J.; Hoekstra, O. S.; Schröder, C. P.; Menke-van der Houven van Oordt, C. W.; Guiot, T.; Brouwers, A. H.; Awada, A.; de Vries, E. G.; Flamen, P. Molecular imaging as a tool to investigate heterogeneity of advanced HER2-positive breast cancer and to predict patient outcome under trastuzumab emtansine (T-DM1): the ZEPHIR trial. *Ann. Oncol.* **2016**, *27* (4), 619−624.
(36) Pereira, P. M. R.; Mandleywala, K.; Ragupathi, A.; Carter, L. M.; Goos, J. A. C. M.; Janjigian, Y. Y.; Lewis, J. S. Temporal Modulation of HER2Membrane Availability Increases Pertuzumab Uptake and Pretargeted Molecular Imaging of Gastric Tumors. *J. Nucl. Med.* **2019**, *60* (11), 1569.

https://doi.org/10.1021/acsomega.3c03614
ACS Omega 2023, 8, 35884−35892